remote sensing

MDPI

Article

Early Detection of Bacterial Wilt in Tomato with Portable Hyperspectral Spectrometer

Yi Cen [1], Ying Huang [2], Shunshi Hu [2,3,*], Lifu Zhang [1] and Jian Zhang [4]

[1] Aerospace Information Research Institute, Chinese Academy of Sciences, Beijing 100101, China; cenyi@radi.ac.cn (Y.C.); zhanglf@aircas.ac.cn (L.Z.)
[2] School of Geographic Sciences, Hunan Normal University, Changsha 410081, China; ying.huang@hunnu.edu.cn
[3] Hunan Key Laboratory of Geospatial Big Data Mining and Application, Changsha 410081, China
[4] Macro Agriculture Research Institute, College of Resource and Environment, Huazhong Agricultural University, 1 Shizishan Street, Wuhan 430070, China; jz@mail.hzau.edu.cn
* Correspondence: shunshi.hu@hunnu.edu.cn

Abstract: As a kind of soil-borne epidemic disease, bacterial wilt (BW) is one of the most serious diseases in tomatoes in southern China, which may significantly reduce food quality and the total amount of yield. Hyperspectral remote sensing can detect crop diseases in the early stages and offers potential for BW detection in tomatoes. Tomatoes in southern China are commonly cultivated in greenhouses or bird nets, limiting the application of remote sensing based on natural sunlight. To resolve these issues, we collected the spectrum of tomatoes firstly using the HS-VN1000B Portable Intelligent Spectrometer, which is equipped with a simulated solar light source. We then proposed a tomato BW detection model based on some optimal spectral features. Specifically, these optimal features, including vegetation indexes and principal components (PCs), were extracted by the sequential forward selection (SFS), the simulated annealing (SA), and the genetic algorithm (GA) and were finally fed into the support vector machine (SVM) classifier to detect diseased tomatoes. The results showed that the infected and healthy tomatoes exhibit different spectral characteristics for both leave and stem spectra, especially for near-infrared bands. In addition, the BW detecting model built by the combination of GA and SVM (GA-SVM) achieved the best performance with overall accuracies (OA) of 90.7% for leaves and 92.6% for stems. Compared with the results based on leaves, spectral features of stems provided better accuracy, indicating that the symptom of early infection of BW is more significant in tomato stems than in leaves. Further, the reliability of the GA-SVM tomato stem model was verified in our 2022 experiment with an OA of 88.6% and an F1 score of 0.80. Our study provides an effective means to detect BW disease of tomatoes in the early stages, which could help farmers manage their tomato production and effectively prevent pesticide abuse.

Keywords: bacterial wilt disease; infection detection; hyperspectral remote sensing; tomato

Citation: Cen, Y.; Huang, Y.; Hu, S.; Zhang, L.; Zhang, J. Early Detection of Bacterial Wilt in Tomato with Portable Hyperspectral Spectrometer. *Remote Sens.* **2022**, *14*, 2882. https://doi.org/10.3390/rs14122882

Academic Editors: Thomas Alexandridis and Saeid Homayouni

Received: 21 March 2022
Accepted: 13 June 2022
Published: 16 June 2022

1. Introduction

Tomato is one of the dominant and most consumed vegetables around the whole world [1], and its growth and production have essential role for people at local and national in terms of socioeconomic development and food security [2]. According to the investigation report [3], China has the largest tomato-planting area and produces tremendous tomato yields in the world, with an annual yield of 65.15 million tons, close to 1/3 of the global tomato production. There are more than 40 kinds of tomato diseases in China, among which more than 10 seriously occurred national wide. Bacterial wilt (BW) disease, caused by *Ralstonia solanacearum* (Smith) Yabuuchi et al., is a pathogenic soil-borne epidemic disease for Solanaceae vegetables [4], which is a serious disease and could cause tomato yield loss of up to 91%. The BW disease transmits implicitly, outbreaks suddenly and spreads quickly through soil and water across the whole farmland under appropriate temperature and

humidity conditions in the plot, resulting in most of the other healthy plants infected with BW soon [5]. Once the BW pathogen enters the xylem of the tomato, it propagates in the vascular bundle and obstructs water and nutrients transportation, causing crown foliage to wilt first and then the entire plant death in a few days, leading to a significant tomato yield reduction. The BW disease is mainly distributed in tropical and subtropical areas and is especially common in southern China [6].

Nowadays, many trials, including cultural practices, soil amendment, fumigation, spraying chemical agents or bactericides, and breeding resistant varieties, have been carried out to control the BW disease [7–9]; however, with no significant achievements [10]. More importantly, misuse and overuse of chemical agents or bactericides could give rise to agricultural soil pollution and bring great pressure to the ecological environment. Therefore, it is important to obtain timely and accurate information about the state of BW disease and spatial distributions to reduce the secondary infection by biological control or even early removing the infected ones [11]. Traditional detection methods of BW disease, such as field investigation, manual discrimination, and chemical testing, are usually time-consuming, inefficient, expensive and even destructive [12]. Hence, advanced and automated BW detection methods with a contactless, nondestructive way are favored for tomato cultivation companies and farmers, which can provide accurate disease information in near real-time [13].

Hyperspectral remote sensing records target spectra with dozens or even hundreds of fine spectral bands and has the ability to discriminate different targets through fine spectral characteristics [14,15], booming prosperous scientific research prospects in many fields, including air pollution monitoring [16], crop fine classification, vegetation biochemical parameter retrieval, crop disease monitoring and early detection [12,17]. In recent decades, it has achieved great improvements both in imaging systems and different application fields [18,19]. For example, in crop disease monitoring and detection fields, it is regarded as an effective way due to its advantages of nondestructive detection and abundant spectral information [20–22]. Numerous studies indicate that it can be used to detect lots of crop diseases, such as pine wilt disease [23], peanut leaf spot [24], early blight disease [25], late blight diseases [25] and etc., highlighting the great potentials on tomato BW. However, most previous studies focused on field crops and tomatoes in southern China are often planted in greenhouses or bird nets, where passive solar-based remote sensing is limited because the solar radiation is declined and affected seriously, and the space room is also restricted. The portable spectrometer with a simulated solar light source, which releases the dependence on natural sunlight, has become a good observation means for practical applications.

The HS-VN1000B Portable Intelligent Spectrometer, produced by Progoo Information Technology Co., Ltd., Tianjin, China, is equipped with a built-in simulated solar light source and can be controlled by a mobile app through a Bluetooth connection. The app uses the cloud big data analysis system to interpret the collected spectrum, and the results can be displayed to customers in real-time. Compared with other spectrometers, HS-VN1000B Portable Intelligent Spectrometer has significant advantages in crop disease detection, such as small volume, high sensitivity, low power consumption, and high-cost performance. With HS-VN 1000B, the observable objects are no longer limited to leaves and canopies but also stems, which often are infected earlier in plants.

Crops spectra between visible and near-infrared spectral ranges can be applied to detect early disease changes caused by biotic stresses because diseases carry different physiological and ontogenetical responses to these spectral bands [26–28]. Though hyperspectral remote-sensing technique can capture the crop's fine spectra within these spectral bands, the collected spectra have high dimensions and most spectral bands are highly relevant to others, which makes it difficult to accurately identify an infected crop. Hence, there are various approaches designed for extracting distinctive spectral features from hyperspectral remote sensing datasets for some specified applications [29–31]. Through feature extraction or feature engineering, the spectra dimensions will be decreased, and the spectra correlations will also be eliminated; thus, the most representative spectral character-

istics are retained, which may highly improve crop disease detection model performance. For example, Elhadi et al. [32] developed a guided regularized random forest (GRRF) method to extract six key features for the early-stage detection of maize crop infected with phaeosphaeria leaf spot (PLS), with an overall accuracy (OA) of 88% and a kappa value of 0.75. Nevertheless, when all spectral bands are included in the model, the classification accuracy, on the contrary, dropped dramatically, with an OA of only 82% and a kappa of 0.64. Nagasubramanian et al. [33] identified the optimal combination of six bands from 240 hyperspectral bands by using genetic algorithms (GA) for early discrimination of charcoal rot disease of soybean stems, and compared to using only RGB bands, the optimal combination of six bands obtained better results in SVM model with an OA of 90.91% and an F1-score of 0.90, which highlights the optimal band combination and the non-visible wavelength for disease detection. Because of the high dimensionality of hyperspectral data, a thorough search for the subset of best features using an enumerate way incurs a tremendous computational burden and thus is impractical.

Heuristic algorithms quickly determine near-optimal solutions to an optimization problem by greatly reducing the number of attempts of try and error in the limited search space, not the entire solution space. Therefore, various heuristic algorithms are emerging and have successfully been applied in feature selection with high dimensions. Sequential forward selection (SFS) [34] with sequential search strategy and simulated annealing (SA) [35] with random search strategy are classic heuristic algorithms and characterized by short running time and easy to implement, so they have a wide range of applications. Genetic algorithms (GA) [36] used with a random search strategy is another kind of heuristic algorithm and have a strong global search capability [37]. Hence, SFS [34], SA [35], and GA [36] were adopted to search for an optimal subset of spectral features in this work to maximize the efficiency and reduce the computational complexity of using hyperspectral data [38].

The extracted features are then usually input into classifiers to determine the crop's healthy status. Support vector machine (SVM) is one of the preferred and classic machine learning-based classifiers and is applied by most scholars worldwide in various scientific research fields [39,40] because it has good generalization capability in few-shot learning with just a few parameters to consider and is less prone to over-fitting. Hence, it is a promising way to develop a crop disease detection model by integrating machine-learning techniques with different feature extraction methods.

Therefore, this study aims to develop a practical monitoring method for the early detection of tomato BW disease using HS-VN1000B Portable Intelligent Spectrometer. This work also tries to discover if plant leaf or stem spectra are more appropriate for early detection of the BW disease in tomatoes.

2. Materials and Methods

2.1. Field Experiments

The study area is located in the Gaoqiao scientific research and experiment base, Hunan Academy of Agricultural Sciences, Hunan Province, China (113.36°E, 28.48°N). Three tomato varieties, namely Ruila, Laixideng and Kaide1832, were planted for spectrum measurement in this study, as they are widely cultivated in China and much more susceptible to being infected with BW disease. Tomato seedlings were raised in March, transplanted on April 5, flowered at the end of April with the fruit setting in May, and most of them died due to bacterial wilt infection in early June. In total, 150 plants were infected with BW disease naturally, and another 50 of them were used as a healthy control group. Compound fertilizer with the amount of 1500 kg per ha was applied before sowing, which consisted of N-P_2O_5-K_2O (17-17-17). The weed and pest control strategies and irrigation management in the experimental field were adjusted according to local agronomic management practices.

2.2. Data Acquisition

2.2.1. Disease Severity Assessment

According to the standards from the book [41] and suggestions from local, experienced tomato planting experts, BW severity could be assessed by the degree of leaf wilting, where 0 represents no leaf wilting, 1 represents top 2–3 leaves wilting, 2 represents all leaves wilting, and 3 represents a dead plant, as shown in Figure 1. However, once the leaves wither, it is difficult to control the disease with chemicals, and the infected plant dies rapidly in a few days. Only the edge of the leaf on the crown curls because of water loss, which occurs in the early stage of tomato BW disease and can be treated using anti-bacterial agents. For this reason, this study mainly focuses on the early detection of tomato BW disease during the curling stage of the top leaves.

Figure 1. Disease severity of tomato BW: (**a**) leaf curling (early detection); (**b**) top leaves wilting (1); (**c**) all leaves wilting (2); (**d**) dead (3).

2.2.2. Reflectance Measurements

The tomato spectrum measure experiments were conducted in BW disease early stages on 7 May, 20 May, 6 June, and 19 June, 2021. The HS-VN1000B Portable Intelligent Spectrometer was used in this study to measure the spectrum of healthy and infected tomatoes, with the instrument parameters shown in Table 1. Figure 2 shows the sketch map for spectrum measurement using HS-VN1000B spectroradiometer. The spectrometer obtained the spectrum by clinging to the measured objects because it provided a built-in light source. The dark current and white reference reflectance are also recorded for reflectance inversion. In order to avoid the influence of stray light on the spectral acquisition, we also used a black shelter with very low reflectance to block the underlying surface. A total of 354 leaf samples and 179 stem samples were collected and processed for modeling, of which 114 were healthy and 240 were infected leaf samples, and 130 were infected and 49 were healthy stem samples.

Table 1. Instrument parameters of HS-VN1000B Portable Intelligent Spectrometer.

Wavelength	400 nm–1000 nm	Spectral	3 nm
Size	<20 × 10 × 4 cm	Weight	<0.58 kg
Bands	300	Light	Built-in halogen lights
Power supply	1 standard 18,650 battery	Data interface	Bluetooth

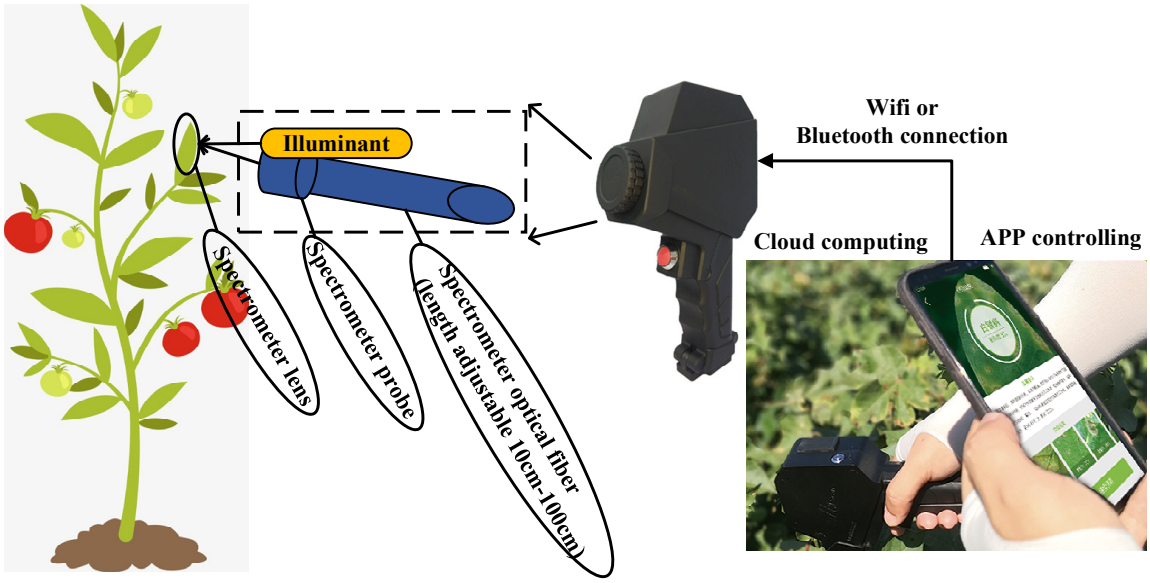

Figure 2. Reflectance measurements using HS-VN1000B Portable Intelligent Spectrometer.

2.3. Data Processing

The workflow of the steps from the reflectance measurements to the disease early detection modelling is presented in Figure 3. Firstly, the raw reflectance of healthy and diseased tomato leaves and stems was obtained by the spectrometer. Then, the raw reflectance was pre-processed to eliminate the spectrum noise. SFS, SA and GA were used as feature selection methods to obtain the optimal subset of features. SVM binary classification method was used to detect the disease. Finally, the model performance was evaluated.

2.3.1. Data Pre-Processing

The Savitzky–Golay (S-G) smoothing filter [42] was used in this study to eliminate the spectrum noise caused by the spectrometer sensitivity. A third-order polynomial with a slide filter window of 3 was applied to further improve the spectral smoothness and data quality [28].

$$Y_j^* = \frac{\sum_{i=-m}^{m} C_i \times Y_{j+i}}{N} \quad (1)$$

where Y_j^* is the fitted value, Y_{j+i} is the original value of the spectrum, C_i is S-G fit polynomial coefficients, obtained by fitting the given higher-order polynomial within a sliding window, m is the width of half the filter, N is the filter length, $N = 2m + 1$.

2.3.2. Extraction of Spectral Data

The high dimensionality of hyperspectral data often makes it contain much redundant information. It is common to use the band selection algorithm to reduce data dimensionality and complexity [37]. Referring to related studies on BW hyperspectral disease detection and water stress [5,26,43], a total of 35 vegetation indices (VIs) (Table 2) and 25 principal components (PCs) were employed to obtain effective spectral features.

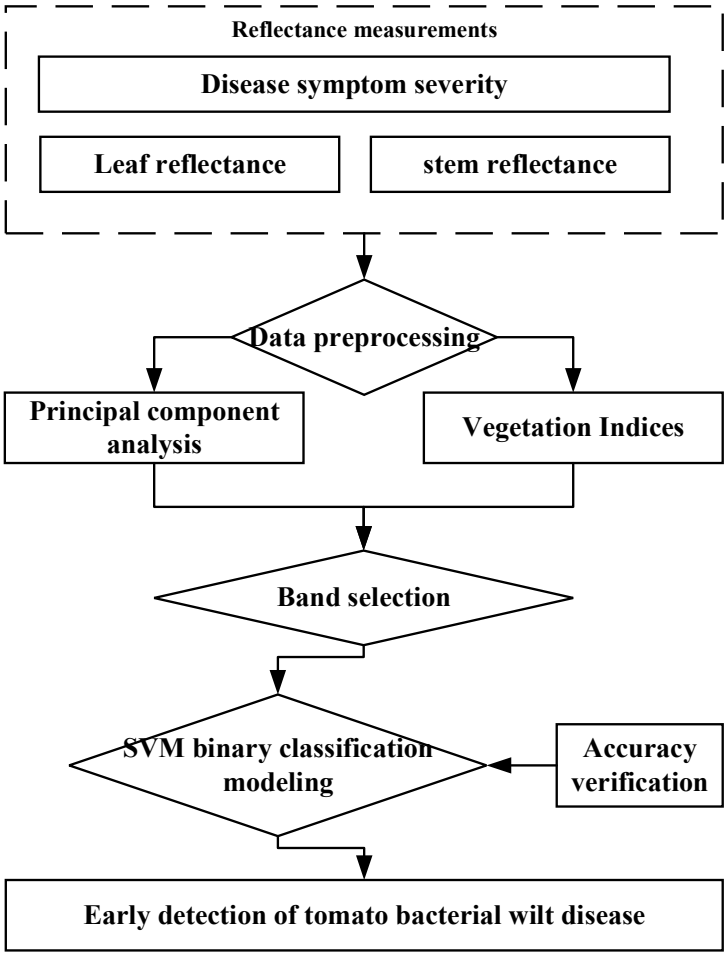

Figure 3. Flowchart of the data processing used in this study.

Table 2. Vegetation indices employed in this study.

Vegetation Index	Equations	Reference
Water Index, WI	R_{900}/R_{970}	[43]
Normalized Water Index, NWI	$(R_{970} - R_{900})/(R_{970} + R_{900})$	[43]
Normalized Water Index, WI:NDVI	$WI/NDVI$	[43]
Normalized Difference Vegetation Index, NDVI	$(R_{800} - R_{670})/(R_{800} + R_{670})$	[43]
Renormalized Difference Vegetation Index, RDVI	$(R_{800} - R_{670})/(R_{800} + R_{670})^{1/2}$	[43]
Optimized Soil Adjusted Vegetation Index, OSAVI	$(1 + 0.16)(R_{800} - R_{670})/(R_{800} + R_{670} + 0.16)$	[43]
Normalized Photochemical Reflectance Index, PRI_{norm}	$PRI/(RDVI * (R_{700}/R_{670}))$	[43]
Photochemical Reflectance Index, PRI_{570}	$(R_{570} - R_{531})/(R_{570} + R_{531})$	[43]
Photochemical Reflectance Index, PRI_{550}	$(R_{550} - R_{531})/(R_{550} + R_{531})$	[43]
Photochemical Reflectance Index 1, PRI1	$(R_{528} - R_{567})/(R_{528} + R_{567})$	[26]
Photochemical Reflectance Index 2	$(R_{531} - R_{570})/(R_{531} + R_{570})$	[26]
Greenness index, G	R_{554}/R_{677}	[26]
Modified Chlorophyll absorption in Reflectance Index, MCARI	$((R_{700} - R_{670}) - 0.2 * (R_{700} - R_{550})) * (R_{700}/R_{670})$	[26]
Transformed CARI, TCARI	$3 * ((R_{700} - R_{670})) - 0.2 * (R_{700} - R_{550})) * (R_{700}/R_{670})$	[26]
Triangular Vegetation Index, TVI	$0.5 * (120 * (R_{750} - R_{550})) - 200 * (R_{670} - R_{550}))$	[26]

Table 2. *Cont.*

Vegetation Index	Equations	Reference
Zarco-Tejada & Miller, ZM	R_{750}/R_{710}	[26]
Simple Ratio Pigment Index, SRPI	R_{430}/R_{680}	[26]
Normalized Phaeophytinization Index, NPQI	$(R_{415}-R_{435})/(R_{415}+R_{435})$	[26]
Normalized Pigment Chlorophyll Index, NPCI	$(R_{680}-R_{430})/(R_{680}+R_{430})$	[26]
Carter Index 1, Ctr1	R_{695}/R_{420}	[26]
Carter Index 2, Ctr2	R_{695}/R_{760}	[26]
Lichtenthaler Index 1, LIC1	$(R_{800}-R_{680})/(R_{800}+R_{680})$	[26]
Lichtenthaler Index 2, LIC2	R_{440}/R_{690}	[26]
Structure Intensive Pigment Index, SIPI	$(R_{800}-R_{450})/(R_{800}+R_{650})$	[26]
Vogelmann Index 1, Vog1	R_{740}/R_{720}	[26]
Vogelmann Index 2, Vog2	$(R_{734}-R_{747})/(R_{715}+R_{726})$	[26]
Vogelmann Index 3, Vog3	$(R_{734}-R_{747})/(R_{715}+R_{720})$	[26]
Gitelson and Merzlyak 1, GM1	R_{750}/R_{550}	[26]
Gitelson and Merzlyak 2, GM2	R_{750}/R_{700}	[26]
Bacterial wilt index1, BWI1	$(R_{790}-R_{650})/2+R_{790}$	[5]
Bacterial wilt index2, BWI2	R_{730}/R_{790}	[5]
Bacterial wilt index3, BWI3	$(R_{790}-R_{580})/2+R_{790}$	[5]
Bacterial wilt index4, BWI4	$(R_{790}-R_{730})/2+R_{790}$	[5]
Bacterial wilt index5, BWI5	$(R_{790}-R_{730})/2-R_{790}$	[5]
Bacterial wilt index6, BWI6	$(R_{790}-R_{650})/2-R_{790}$	[5]

2.3.3. Band Selection

Disease detection using a hyperspectral remote sensing technique generally involves building features representing disease spectral response. However, not all of these features are equally significant for a specific task [44]. The selection of fewer but effective and optimal bands is widely employed for developing a crop disease detection model with the aim to improve robustness, accuracy and computational effectiveness [45]. Three feature selection methods (SFS, SA and GA) were adopted to get the optimal subset of spectral features. All the data processing and the implementation of the disease detection model were conducted using PyCharm software (python v3.6), version 2019 by JetBrains from the Czech Republic.

The SFS algorithm progressively adds features according to a "bottom-up" search strategy starting from the empty set until as many features as required are selected [46]. The method takes inter-feature combinations into account to some extent [47], however, it can not remove the selected features, even if they decrease the accuracy of the model.

SA is one of the heuristic methods for feature optimization in hyperspectral data [35,48]. It randomly selects a feature subset from the current optimal feature subset. In case the new feature subset performs better, the new subset will be adopted to replace the current optimal feature subset. In the case that the new feature subset performs poorly, it will still be adopted with a certain probability, which depends on the current state (temperature) [35]. The detailed SA process is described by Gheyas and Smith [49].

GA is based on the random global search optimization strategy and evaluation criteria to obtain an optimal subset of features [50]. By randomly generating the chromosomes and encoding each chromosome into one set of feature combinations, which undergo successive iterations of selection crossover and mutation genetic operators to generate new chromosomes with better fitness values, the final chromosome with the largest fitness value is the optimal solution for that feature dimension. Considering the dependency between the features, GA can extract important features with sufficient information and give a better optimal solution [31]. Compared with GA, features selected by SFS each time are not removed, limiting combinatorial solutions of features considered, and the poor global search ability of SA makes it vulnerable to other parameters [51].

The SVM classifier shows lots of unique advantages in solving small samples, non-linear, and high-dimensional pattern recognition [52]. Hence, we adopted the SVM clas-

sifier in this study, and the radial basis function (RBF) kernel was employed because of its high performance [17,53–55]. The grid search strategy was used to optimize SVM hyper-parameters.

The samples were randomly divided into training (70%) and test (30%) groups and 10-fold cross-validation was applied to evaluate their performance. The accuracy criteria such as recall, precision, F1 score, and OA, shown in Equations (2) to (5), were employed. In these formulas, TP means true and correctly classified, TN means true but classified wrong, while FP means false but classified to be true, and FN means false and correctly classified [56]. Additionally, the F1 score can address the problem of unbalanced class distribution better than OA because it is precise and simultaneously recalls into account [57]. If the F1 score is closer to 0, the poorer the model performance is, while if it is closer to 1, the better the model performance is.

$$\text{Recall} = \frac{\text{TP}}{\text{TP} + \text{FN}} \tag{2}$$

$$\text{Precision} = \frac{\text{TP}}{\text{FP} + \text{TP}} \tag{3}$$

$$\text{F1 Score} = 2 \cdot \frac{\text{Recall} \cdot \text{Precision}}{\text{Recall} + \text{Precision}} \tag{4}$$

$$\text{OA} = \frac{\text{TP} + \text{TN}}{\text{TP} + \text{TN} + \text{FP} + \text{FN}} \tag{5}$$

2.3.4. Data Analysis

The spectral reflectance curves of all healthy and infected tomatoes obtained from the four experiments (7 May, 20 May, 6 June, 19 June) are shown in Figure S1 (in Supplementary Materials). It could be concluded that the overall shape of the spectral reflectance of healthy plants is similar to infected plants, increasing from 438 nm to 550 nm, subsequently dropping until 680 nm, followed by a sharp increase after 765 nm. Compared with infected plants, the healthy ones presented the higher leaf and stem reflectance values in the NIR region. This is because the physiological stress caused by the pathogen invasion has a certain influence on the internal structure of plant leaf and stem, diminishing their internal reflective capacity, thus causing a reduction in reflection of NIR energy [26]. Compared with leaf reflectance, the stem reflectance of healthy and infected plants presented a more significant difference, and it might be because this study mainly focuses on the early infected stage, while the water shortage in leaves is slight, but the stem has already been infected.

3. Results

For the same feature optimization method, the combination of features with high fitness value may have higher classification accuracy than that of features with low fitness value. Therefore, we select the optimal feature combination corresponding to the maximum fitness value as the input variables to the SVM classifier. It was found in Figure 4 that there were 16, 22, and 10 spectral leaf features and 20, 12 and 10 stem spectral features selected by SFS, SA and GA, respectively. For the optimal feature subset of tomato leaves and stems, it was noticed that GA selected the least number of spectral features and on the other hand, SFS selected a relatively larger number of spectral features, which was associated with the inability of the SFS algorithm to delete the features that had been already chosen earlier. Details of the results from the optimal feature subsets selected by the three feature selection methods are described in Table S1 (in Supplementary Materials). Figure 5 shows the spectral features selected by SFS, SA and GA, which have a correlation greater than 50%. The SRPI has the greatest contribution in all of the disease detection models based on tomato leaf spectra, which could be explained by the fact that it indicates the changes in nitrogen content and photosynthetic efficiency in infected tomatoes. Among the tomato stem disease detection models, PC13 showed a greater contribution, which further

demonstrated that the PCs with small variance might be more effective in disease detection. Table 3 shows the results that examine the separation ability of features for healthy and diseased samples using an independent *t*-test. The mean and standard deviation of all VIs were significantly different between the healthy and diseased samples, and it was significant at the 0.99 level for all features selected by the three feature selection methods.

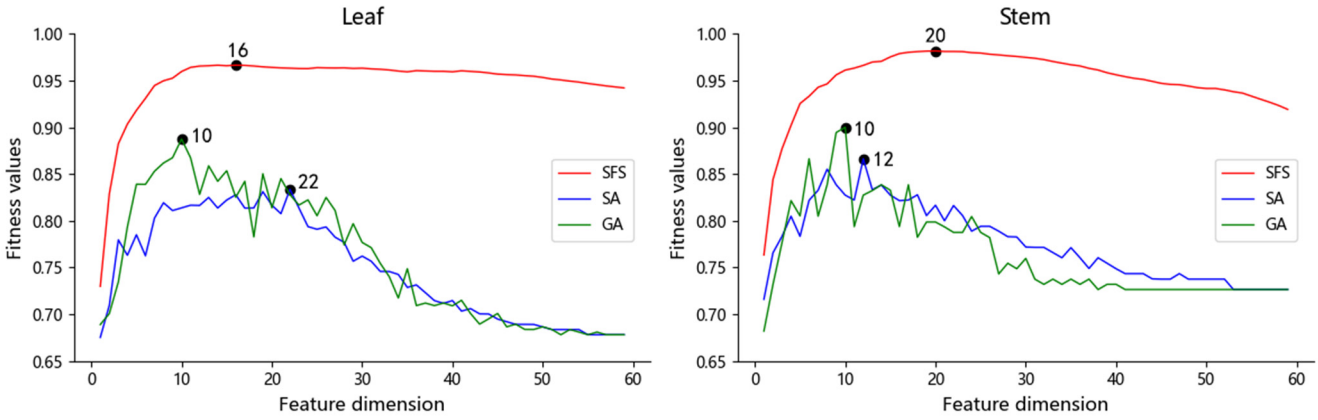

Figure 4. The optimal feature combination selection results of SFS, SA and GA in any feature dimension: (**a**) results for the optimal feature combinations of tomato leaves; (**b**) results for the optimal feature combinations of tomato stems.

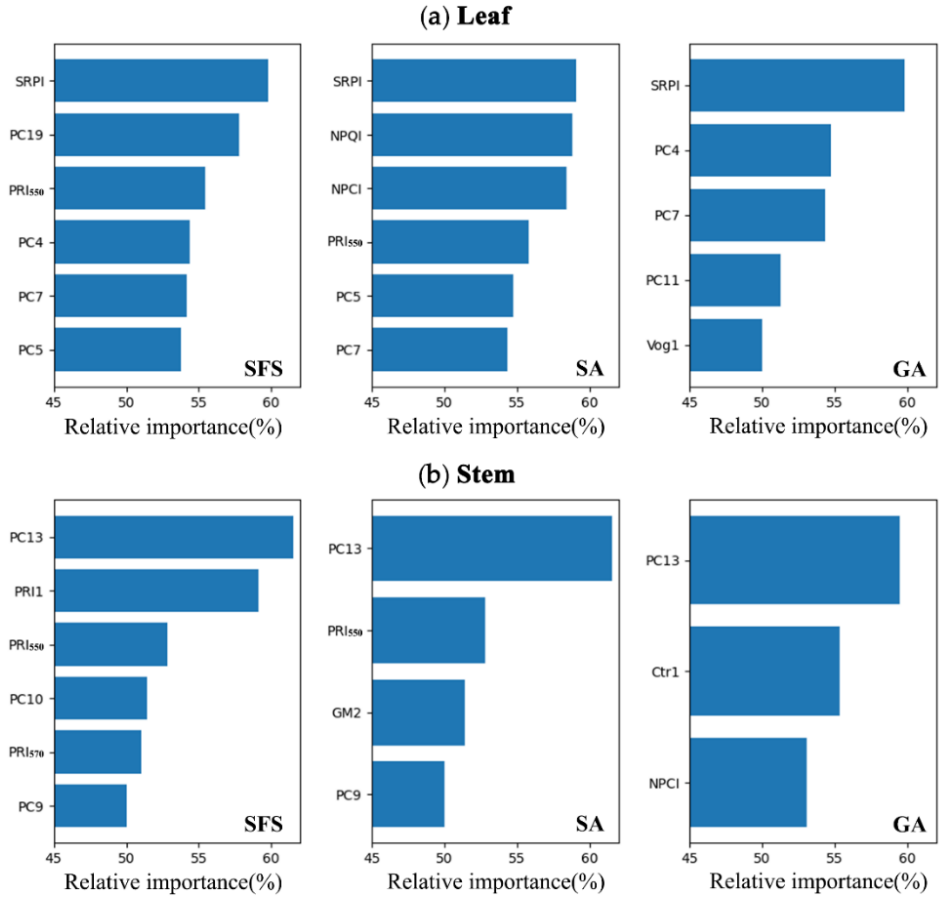

Figure 5. The SFS, SA and GA selected spectral features that were input to the SVM and the relative importance greater than 50% were output: (**a**) relative importance of spectral features of tomato leaves model; (**b**) the relative importance of spectral features of tomato stems model.

Table 3. Summary statistics of VIs selected by feature selection methods.

Methods	Leaf/Stem	Features	Mean		Standard Deviations		Significance of *t*-Test
			Healthy	Diseased	Healthy	Diseased	
SFS	Leaf	PRI550	0.045	0.040	0.010	0.010	**
		Vog1	1.472	1.479	0.079	0.081	**
		Vog2	−0.082	−0.084	0.016	0.018	**
		Ctr2	0.212	0.218	0.026	0.027	**
		SRPI	1.039	0.955	0.123	0.103	**
	Stem	PRI550	0.040	0.046	0.006	0.008	**
		WI	1.174	1.169	0.020	0.022	**
		WI:NDVI	1.726	1.757	0.104	0.103	**
		PRI570	−0.011	0.001	0.011	0.016	**
		BWI2	0.904	0.915	0.020	0.016	**
		G	1.859	1.920	0.188	0.199	**
		PRI1	−0.017	−0.027	0.008	0.014	**
		LIC1	0.660	0.644	0.036	0.040	**
		GM1	2.803	2.578	0.436	0.310	**
SA	Leaf	PRI550	0.045	0.040	0.010	0.010	**
		OSAVI	0.719	0.702	0.033	0.034	**
		NPCI	−0.016	0.026	0.049	0.052	**
		SIPI	0.771	0.754	0.031	0.033	**
		PRI570	−0.059	−0.054	0.025	0.021	**
		ZM	2.174	2.193	0.175	0.192	**
		SRPI	1.039	0.955	0.123	0.103	**
		NPQI	0.017	0.003	0.016	0.022	**
		PRI1	0.013	0.014	0.022	0.018	**
		Ctr2	0.212	0.218	0.026	0.027	**
		Vog2	−0.082	−0.084	0.016	0.018	**
		Vog3	−0.090	−0.092	0.019	0.020	**
		GM2	3.579	3.531	0.415	0.409	**
	Stem	PRI550	0.040	0.046	0.006	0.008	**
		RDVI	0.550	0.544	0.040	0.04	**
		WI	1.174	1.169	0.020	0.022	**
		LIC1	0.660	0.644	0.036	0.040	**
		Vog2	−0.031	−0.027	0.006	0.006	**
		Vog3	−0.032	−0.028	0.006	0.006	**
		GM2	2.085	1.950	0.188	0.199	**
GA	Leaf	SRPI	1.039	0.955	0.123	0.103	**
		Vog1	1.472	1.479	0.079	0.081	**
		Ctr2	0.212	0.218	0.026	0.027	**
	Stem	NWI	−0.080	−0.078	0.009	0.009	**
		WI:NDVI	1.726	1.757	0.104	0.103	**
		PRI2	0.011	−0.001	0.011	0.016	**
		NPCI	0.154	0.172	0.045	0.057	**
		Ctr1	2.472	2.659	0.279	0.354	**
		GM1	2.803	2.578	0.436	0.310	**

Note: ** indicates that the mean differences are significant at the 0.99 levels.

The optimal features selected by SFS, SA and GA methods were fed into SVM classifier to identify infected and healthy tomatoes. We developed six early detection models based on the spectral features of leaves and stems using different feature selection methods. The OA and F1 score criteria of the six models are presented in Table 4. BW disease detection models based on leaf spectrum using SFS, SA, and GA methods resulted in an OA of 89.7%, 86.0%, and 90.7%, with F1 scores of 0.83, 0.79, and 0.85, respectively. The BW disease detection models based on stem spectrum using SFS, SA, and GA methods resulted in an OA of 92.6%, 88.9%, and 92.6%, and F1 scores of 0.85, 0.80, and 0.87, respectively.

Comparing the model performances for different optimal feature combinations, GA showed the best performance, followed by SFS, while SA showed the worst performance for the SVM model. Overall, the SVM built with the optimal subset of features that were selected by GA as input variables achieved the best performance on 10-fold cross-validation, with F1 scores of 0.85 for leaves and 0.87 for stems.

Table 4. SVM built with different feature selection methods for comparative performance of tomato disease detection models.

Feature Selection Methods	Leaf/Stem	Healthy (%)	Diseased (%)	Overall Accuracy (%)	F1 Score
SFS	Leaf	76.5	95.9	89.7	0.83
	Stem	78.6	97.5	92.6	0.85
SA	Leaf	82.4	87.7	86.0	0.79
	Stem	85.7	90.0	88.9	0.80
GA	Leaf	85.3	93.2	90.7	0.85
	Stem	92.9	92.5	92.6	0.87

4. Discussion

To investigate the reliability of the GA-SVM model for identifying tomato BW, the experiment was replicated on 13 May 2022, at GeNongJiang Agricultural Products Co., Ltd. in Changsha, Hunan Province, China (location: 113.41°E, 28.08°N;) (Figure 6). Types T101 and T106 of tomatoes were sown at 45 cm × 45 cm seed spacing on 26 December 2021 and grafted on 28 March 2022, with 400 grafted tomatoes that were not susceptible to BW and 200 ungrafted tomatoes that were extremely susceptible to BW. The total planting area was 200 m^2. A fertilizer compound that contains 7.5 kg of N, P_2O_5, and K_2O, respectively, was applied as the base fertilizer before sowing and followed up with drip irrigation once after sowing. Weeds and pests were controlled according to local agronomic measures. In May 2022, about 8% of the tomatoes naturally developed BW (BW was visible in the greenhouse); hence, the experiment was conducted on 13 May 2022.

Figure 6. Tomato experimental field of GeNongJiang Agricultural Products Co., Ltd. in Changsha, Hunan Province, China (location: 113.41°E, 28.08°N).

The HS-VN1000B spectroradiometer was applied to acquire the tomato stem spectra with a black mask with low reflectance to obstruct the underlying surface. Thirty-five tomato stem samples were taken as input to the GA-SVM model, of which 25 were infected plants and 10 were healthy plants. The results demonstrated that the OA was 88.6%, and the F1 score was 0.80 (Table 5). Considering the variations in location, time, and environment

of the 2022 experiment, the results were considered reasonable and validated the usefulness and reliability of the GA-SVM tomato stem model. Figure S2 (in Supplementary Material) presents the spectral stem curves of all healthy and diseased plants in the 2022 experiment.

Table 5. The validation results of the GA-SVM model for the 2022 experiment.

Predicted / True	Healthy	Diseased	Healthy (%)	Diseased (%)	Overall Accuracy (%)	F1 Score
Healthy	8	2	80.0	92.0	88.6	0.80
Diseased	2	23				

In this work, we developed tomato BW disease detection models using HS-VN1000B Portable Intelligent Spectrometer. Since the equipment has a built-in light and is no longer limited by external light source conditions, it can be well used outdoors with cloudy and rainy weather or in facilities like greenhouses and bird nets. Furthermore, a more stable spectrum can be obtained effectively by HS-VN1000B without considering the observation angle of the ground objects. The instrument is small and light, convenient for carrying, and the operation based on the mobile app is simple, which means it is also suitable for ordinary people without a professional background. Through a 5G wireless network, the spectrum can be analyzed and shown in a mobile app in real-time using the disease detection model of the big data cloud platform. The equipment meets the requirements of real-time, nondestructive, and accurate detection of crop diseases and provides a new application perspective for the development of precision agriculture.

The phytopathology of this disease has been deeply studied as well as the traits of the infected plants. When a tomato plant is infected with BW disease, these bacteria spread into the crown and stem through the plant's vascular system in a few hours [58]. It may cause wilt in plants by invading through the xylem vessels and colonizing the xylem, preventing water movement into the upper portion of plant tissues and damaging tissue and cell structure inside the plant. The spectral responses caused by BW disease in tomato are highly correlated with these physiological and ontogenetical factors and shows a reduced spectral reflection in the NIR region, just like the research work findings on Brinjal [26]. It is interesting that this phenomenon is clearly observed between infected and healthy tomatoes, regardless of the leaf or stem spectrum, as shown in Figure S1 (in supplementary materials). BW is a soil-borne bacterial disease and it represents a faster bacteria response in vascular bundle blockage than in leaves lacking water. Once infected with BW, the stem of a tomato exhibits special symptoms before leaves showing slight water shortage, wilt traits, as well as damage to cellular structures, such as the proliferation of adventitious roots or buds in the middle or lower parts of the infected stems.

Since early detection of BW disease in tomatoes is important for its production and management, it is expected to adopt some sensitive spectral futures representing disease symptoms in the early stages to achieve this goal. Fortunately, the performance of the early disease detection model based on stem reflectance outperforms that of leaf reflectance, with the highest OA (92.6%) and F1 Score (0.87) by GA-SVM for the 2021 experiment and nice OA (88.6%) and F1 score (0.80) for GA-SVM for the 2022 experiment. It provides evidence of the feasibility and effectiveness of stem monitoring for detecting disease at an early stage. It also highlights that except for the spectrum of leaves and canopy of tomato, the spectrum of the stem provides a promising way for early detecting BW in tomatoes. The findings may help to support the timely control of this vegetation disease in the greenhouse.

Our study successfully applied feature selection methods and machine learning algorithms in an early BW disease detection model for tomato leaves and stems. We obtained an F1 score of 0.85 for the leaves and 0.87 for the stems in our 2021 experiment using optimal spectral features selected by GA. We verified the reliability of applying the GA-SVM model in tomato stems in the 2022 experiment. Three feature selection methods (SFS, SA and GA) decreased the total number of spectral features by over 63%. It is noticeable that in

the leaf model, SRPI, the VI selected by SFS, SA and GA, had the largest contribution in the SVM model, which was probably caused by the xylem blockage in the early infected plants, which obstructed the flow of water and nutrients, leading to the modification of SRPI which is sensitive to leaf nitrogen content [59] and photosynthetic efficiency [60].

In stem models, PC13 with low variance rather showed the largest contribution in the SVM model, which indicates the PCs with low variance may be more vulnerable to changes and possess stronger disease discrimination power. This finding is consistent with the idea proposed by Kuncheva et al. [61]. In the leaf and stem models, it was found that almost all of the optimal feature subsets selected by GA could be found in SFS and SA. Moreover, the best result is obtained by GA-SVM, followed by SFS-SVM and the worst by SA-SVM. It indicates that GA is more capable of searching for the optimal solution globally compared to SFS and SA, while SFS and SA more easily drop into the optimal local solution and are limited by the information redundancy.

In this study, only spectrum features of tomatoes are extracted for building an early BW detecting model. However, the spectral shapes between healthy and infected tomatoes are similar, and there are also spectrum overlapping between each other, which brings big challenges for early BW detection in tomatoes. When a tomato plant is infected with BW disease, the leaves on the crown of the plant are prone to wilt. Obviously, it could induce texture changes in digital camera images. In previous studies that used hyperspectral imagery to monitor crop disease, spectral and texture features were used simultaneously to develop the disease detection model, which achieved good performance [62–64]. Considering the high cost and complex data processing of hyperspectral imagery equipment, spectral information of portable spectrometer and the texture information of mobile phone photos, obtained synchronously by mobile app, will be used to conduct whole period monitoring of tomato BW in the following research.

5. Conclusions

In this study, tomato BW in the early stage was identified using HS-VN1000B Portable Intelligent Spectrometer. The spectrometer was equipped with a built-in simulated solar light source and could be applied in different conditions without natural light limitations. Band selection methods, such as SFS, SA, and GA, were used here to search for the optimal feature set based on spectral features, including PCs and VIs. An SVM classifier model with selected optimal features was created to identify the infected tomatoes. SRPI was found to have the largest contribution in the model based on the leaves' spectrum, which is sensitive to leaf nitrogen content and photosynthetic efficiency. In the model based on the stem's spectrum, PC13 showed the largest contribution, which indicates that PCs with low variance may possess stronger disease discrimination power. The model's performance showed that early detection of BW can be effectively realized by using either stem or leaf spectrum; however, the GA-SVM model based on stem monitoring provides a better result with OA of 92.6% and F1 score of 0.87 in the 2021 experiment and an OA of 88.6% and an F1 score of 0.80 in the 2022 experiment. This is evidence of the feasibility and effectiveness of stem monitoring for detecting tomato BW at an early stage. In the following work, we will explore the possibility of using a combination of spectral features of the portable spectrometer and the texture features of mobile phone photos obtained by mobile app synchronously to monitor a whole period of tomato BW.

Supplementary Materials: The following supporting information can be downloaded at: https://www.mdpi.com/article/10.3390/rs14122882/s1, Figure S1: Comparison between spectra of healthy and diseased tomato in Hunan Province, China, 2022: (a) spectra of healthy and diseased tomato leaf; (b) spectra of healthy and diseased tomato stem; Table S1: Results of SFS, SA and GA to select the optimal subset of features; Figure S2. Comparison between spectra of healthy and diseased tomato stems of experimental tomato field, 2022.

Author Contributions: Conceptualization, Y.C. and S.H.; methodology, Y.C.; software, Y.H.; validation, Y.C., Y.H.; formal analysis, S.H.; investigation, Y.H. and S.H.; writing—original draft preparation,

Y.C. and S.H.; writing—review and editing, S.H.; supervision, J.Z.; project administration, L.Z.; funding acquisition, Y.C. and S.H. All authors have read and agreed to the published version of the manuscript.

Funding: This research was funded by the National Key R&D Program of China (No. 2017YFE0194900); scientific research project supported by Hunan Provincial Education Department (No. 21B0046); 2019 Hunan Postgraduate High-Quality Course Project "Microwave and Hyperspectral Remote Sensing" (No. 130).

Acknowledgments: The authors wish to thank Hunan Vegetable Research Institute personnel, particularly Zhanhong Zhang, Zhanbing Bai, and Xian Ouyang, for providing health and infected samples. We also want to thank Progoo Information Technology Co., Ltd, Tianjin, China, personnel, particularly Xuejian Sun and Yao Huang, for providing two HS-VN1000B Portable Intelligent Spectrometers.

Conflicts of Interest: The authors declare no conflict of interest.

References

1. Asgarian, A.; Soffianian, A.; Pourmanafi, S. Crop type mapping in a highly fragmented and heterogeneous agricultural landscape: A case of central Iran using multi-temporal Landsat 8 imagery. *Comput. Electron. Agric.* **2016**, *127*, 531–540. [CrossRef]
2. Moola, W.S.; Bijker, W.; Belgiu, M.; Li, M. Vegetable mapping using fuzzy classification of Dynamic Time Warping distances from time series of Sentinel-1A images. *Int. J. Appl. Earth Obs. Geoinf.* **2021**, *102*, 102405. [CrossRef]
3. Analysis Report on Production and Marketing Situation and Future Prospect of China's Tomato Industry from 2022 to 2028; R898946. Available online: https://www.chyxx.com/research/202010/898946.html (accessed on 18 January 2022).
4. Chiwaki, K.; Nagamori, S.; Inoue, Y. Predicting Bacterial Wilt Disease of Tomato Plants using Remotely Sensed Thermal Imagery. *J. Agric. Meteorol.* **2005**, *61*, 153–164. [CrossRef]
5. Chen, T.T.; Yang, W.G.; Zhang, H.J.; Zhu, B.Y.; Zeng, R.E.; Wang, X.Y.; Wang, S.B.; Wang, L.D.; Qi, H.X.; Lan, Y.B.; et al. Early detection of bacterial wilt in peanut plants through leaf-level hyperspectral and unmanned aerial vehicle data. *Comput. Electron. Agric.* **2020**, *177*, 105708. [CrossRef]
6. Gaofei, J.; Zhong, W.; Jin, X.; Huilan, C.; Yong, Z.; Xiaoman, S.; Macho, A.P.; Wei, D.; Boshou, L. Bacterial Wilt in China: History, Current Status, and Future Perspectives. *Front. Plant Sci.* **2017**, *8*, 1549. [CrossRef]
7. Tian, J.H.; Rao, S.; Gao, Y.; Lu, Y.; Cai, K.Z. Wheat straw biochar amendment suppresses tomato bacterial wilt caused by Ralstonia solanacearum: Potential effects of rhizosphere organic acids and amino acids. *J. Integr. Agric.* **2021**, *20*, 2450–2462. [CrossRef]
8. Shen, G.H.; Zhang, S.T.; Liu, X.J.; Jiang, Q.P.; Ding, W. Soil acidification amendments change the rhizosphere bacterial community of tobacco in a bacterial wilt affected field. *Appl. Microbiol. Biotechnol.* **2018**, *102*, 9781–9791. [CrossRef]
9. Vu, T.T.; Kim, H.; Tran, V.K.; Vu, H.D.; Hoang, T.X.; Hang, J.W.; Choi, Y.H.; Jang, K.S.; Choi, G.J.; Kim, J.C. Antibacterial activity of tannins isolated from Sapium baccatum extract and use for control of tomato bacterial wilt. *PLoS ONE* **2017**, *12*, e0181499. [CrossRef]
10. Wang, J.; Long, S.F.; Wang, Z.W.; Chen, J.W.; Jiang, F.Y.; Xing, L.I. Research Progress in Controlling Tomato Bacterial Wilt. *China Veg.* **2020**, *1*, 22–30.
11. Chavez, P.; Yarleque, C.; Loayza, H.; Mares, V.; Hancco, P.; Priou, S.; Marquez, M.D.; Posadas, A.; Zorogastua, P.; Flexas, J.; et al. Detection of bacterial wilt infection caused by Ralstonia solanacearum in potato (*Solanum tuberosum* L.) through multifractal analysis applied to remotely sensed data. *Precis. Agric.* **2012**, *13*, 236–255. [CrossRef]
12. Xie, C.Q.; Shao, Y.N.; Li, X.L.; He, Y. Detection of early blight and late blight diseases on tomato leaves using hyperspectral imaging. *Sci. Rep.* **2015**, *5*, 16564. [CrossRef] [PubMed]
13. Mahlein, A.K.; Kuska, M.T.; Behmann, J.; Polder, G.; Walter, A. Hyperspectral Sensors and Imaging Technologies in Phytopathology: State of the Art. *Annu. Rev. Phytopathol.* **2018**, *56*, 535–558. [CrossRef] [PubMed]
14. Xue, Y.; Tong, Q.; Zhang, L. Progress in Hyperspectral Remote Sensing Science and Technology in China Over the Past Three Decades. *IEEE J. Sel. Top. Appl. Earth Obs. Remote Sens.* **2014**, *7*, 70–91.
15. Goetz, A.; Vane, G.; Solomon, J.E.; Rock, B.N. Imaging spectrometry for Earth remote sensing. *Science* **1985**, *228*, 1147–1153. [CrossRef] [PubMed]
16. Cotrozzi, L.; Townsend, P.A.; Pellegrini, E.; Nali, C.; Couture, J.J. Reflectance spectroscopy: A novel approach to better understand and monitor the impact of air pollution on Mediterranean plants. *Environ. Sci. Pollut. Res. Int.* **2018**, *25*, 8249–8267. [CrossRef]
17. Rumpf, T.; Mahlein, A.K.; Steiner, U.; Oerke, E.C.; De Hne, H.W.; Plümer, L. Early detection and classification of plant diseases with Support Vector Machines based on hyperspectral reflectance. *Comput. Electron. Agric.* **2010**, *74*, 91–99. [CrossRef]
18. Zhong, Y.; Hu, X.; Luo, C.; Wang, X.; Zhao, J.; Zhang, L. WHU-Hi: UAV-borne hyperspectral with high spatial resolution (H2) benchmark datasets and classifier for precise crop identification based on deep convolutional neural network with CRF. *Remote Sens. Environ.* **2020**, *250*, 112012. [CrossRef]
19. Bock, C.H.; Poole, G.H.; Parker, P.E.; Gottwald, T.R. Plant Disease Severity Estimated Visually, by Digital Photography and Image Analysis, and by Hyperspectral Imaging. *Crit. Rev. Plant Sci.* **2010**, *29*, 59–107. [CrossRef]

20. Zhang, N.; Yang, G.; Pan, Y.; Yang, X.; Chen, L.; Zhao, C. A Review of Advanced Technologies and Development for Hyperspectral-Based Plant Disease Detection in the Past Three Decades. *Remote Sens.* **2020**, *12*, 3188. [CrossRef]
21. Thomas, S.; Kuska, M.T.; Bohnenkamp, D.; Brugger, A.; Alisaac, E.; Wahabzada, M.; Behmann, J.; Mahlein, A.-K. Benefits of hyperspectral imaging for plant disease detection and plant protection: A technical perspective. *J. Plant Dis. Prot.* **2017**, *125*, 5–20. [CrossRef]
22. Terentev, A.; Dolzhenko, V.; Fedotov, A.; Eremenko, D. Current State of Hyperspectral Remote Sensing for Early Plant Disease Detection: A Review. *Sensors* **2022**, *22*, 757. [CrossRef] [PubMed]
23. Li, F.D.; Liu, Z.Y.; Shen, W.X.; Wang, Y.; Wang, Y.L.; Ge, C.K.; Sun, F.G.; Lan, P. A Remote Sensing and Airborne Edge-Computing Based Detection System for Pine Wilt Disease. *IEEE Access* **2021**, *9*, 66346–66360. [CrossRef]
24. Chen, T.T.; Zhang, J.L.; Chen, Y.; Wan, S.B.; Zhang, L. Detection of peanut leaf spots disease using canopy hyperspectral reflectance. *Comput. Electron. Agric.* **2019**, *156*, 677–683. [CrossRef]
25. Gold, K.M.; Townsend, P.A.; Chlus, A.; Herrmann, I.; Couture, J.J.; Larson, E.R.; Gevens, A.J. Hyperspectral Measurements Enable Pre-Symptomatic Detection and Differentiation of Contrasting Physiological Effects of Late Blight and Early Blight in Potato. *Remote Sens.* **2020**, *12*, 286. [CrossRef]
26. Srivastava, A.; Roy, S.; Kimothi, M.M.; Kumar, P.; Sehgal, S.; Mamatha, S.; Ray, S.S. Detection of bacterial wilt disease (*Pseudomonas solancearum*) in Brinjal using hyperspectral remote sensing. *Int. Arch. Photogramm. Remote Sens. Spat. Inf. Sci.* **2019**, *XLII–3/W6*, 515–520. [CrossRef]
27. Mahlein, A.K. Plant Disease Detection by Imaging Sensors—Parallels and Specific Demands for Precision Agriculture and Plant Phenotyping. *Plant Dis.* **2016**, *100*, 241–251. [CrossRef] [PubMed]
28. Cotrozzi, L. Spectroscopic detection of forest diseases: A review (1970–2020). *J. For. Res.* **2021**, *33*, 21–38. [CrossRef]
29. Maghsoudi, Y.; Valadan Zoej, M.J.; Collins, M. Using class-based feature selection for the classification of hyperspectral data. *Int. J. Remote Sens.* **2011**, *32*, 4311–4326. [CrossRef]
30. Koedsin, W.; Vaiphasa, C. Discrimination of Tropical Mangroves at the Species Level with EO-1 Hyperion Data. *Remote Sens.* **2013**, *5*, 3562–3582. [CrossRef]
31. Li, S.J.; Wu, H.; Wan, D.S.; Zhu, J.L. An effective feature selection method for hyperspectral image classification based on genetic algorithm and support vector machine. *Knowl. -Based Syst.* **2011**, *24*, 40–48. [CrossRef]
32. Elhadi, A.; Houtao, D.; John, O.; Abdel-Rahman, E.M.; Onisimo, M. Detecting the Early Stage of Phaeosphaeria Leaf Spot Infestations in Maize Crop Using In Situ Hyperspectral Data and Guided Regularized Random Forest Algorithm. *J. Spectrosc.* **2017**, *2017*, 691387. [CrossRef]
33. Nagasubramanian, K.; Jones, S.; Sarkar, S.; Singh, A.K.; Singh, A.; Ganapathysubramanian, B. Hyperspectral band selection using genetic algorithm and support vector machines for early identification of charcoal rot disease in soybean stems. *Plant Methods* **2018**, *14*, 86. [CrossRef] [PubMed]
34. Imani, M.; Ghassemian, H. Fast feature selection methods for classification of hyperspectral images. In Proceedings of the International Symposium on Telecommunications, Sydney, Australia, 27–29 April 2015.
35. Serpico, S.B.; Bruzzone, L. A new search algorithm for feature selection in hyperspectral remote sensing images. *Geosci. Remote Sens. IEEE Trans.* **2001**, *39*, 1360–1367. [CrossRef]
36. Li, Q.; Wong, F.; Fung, T. Comparison Feature Selection Methods for Subtropical Vegetation Classification with Hyperspectral Data. In Proceedings of the IGARSS 2019—2019 IEEE International Geoscience and Remote Sensing Symposium, Yokohama, Japan, 28 July–2 August 2019.
37. Huang, X.; Wu, L.; Ye, Y. A Review on Dimensionality Reduction Techniques. *Int. J. Pattern Recognit. Artif. Intell.* **2019**, *33*, 1950017. [CrossRef]
38. Ng, W.; Minasny, B.; Malone, B.P.; Sarathjith, M.C.; Das, B.S. Optimizing wavelength selection by using informative vectors for parsimonious infrared spectra modelling. *Comput. Electron. Agric.* **2019**, *158*, 201–210. [CrossRef]
39. Be Lousov, A.I.; Verzakov, S.A.; Frese, J.V. A flexible classification approach with optimal generalisation performance: Support vector machines. *Chemom. Intell. Lab. Syst.* **2002**, *64*, 15–25. [CrossRef]
40. Mercier, G.; Lennon, M. Support vector machines for hyperspectral image classification with spectral-based kernels. In Proceedings of the IEEE International Geoscience & Remote Sensing Symposium, Toulouse, France, 21–25 July 2003.
41. Li, X.; Du, Y. *Description Standard and Data Standard of Tomato Germplasm*; China Agricultural Press: Beijing, China, 2006.
42. Steinier, J.; Termonia, Y.; Deltour, J. Smoothing and differentiation of data by simplified least square procedure. *Anal. Chem.* **1972**, *44*, 1906–1909. [CrossRef]
43. Ihuoma, S.O.; Madramootoo, C.A. Sensitivity of spectral vegetation indices for monitoring water stress in tomato plants. *Comput. Electron. Agric.* **2019**, *163*, 104680. [CrossRef]
44. Ding, S. Spectral and Wavelet-based Feature Selection with Particle Swarm Optimization for Hyperspectral Classification. *J. Softw.* **2011**, *6*, 1248–1256. [CrossRef]
45. Zhang, X.; Liu, F.; He, Y.; Gong, X. Detecting macronutrients content and distribution in oilseed rape leaves based on hyperspectral imaging. *Biosyst. Eng.* **2013**, *115*, 56–65. [CrossRef]
46. Marcano-Cedeo, A.; Quintanilla-Domínguez, J.; Cortina-Januchs, M.G.; Andina, D. Feature selection using Sequential Forward Selection and classification applying Artificial Metaplasticity Neural Network. In Proceedings of the IECON 2010—36th Annual Conference on IEEE Industrial Electronics Society, Glendale, AZ, USA, 7–10 November 2010.

47. Gao, Z.; Shao, Y.; Xuan, G.; Wang, Y.; Liu, Y.; Han, X. Real-time hyperspectral imaging for the in-field estimation of strawberry ripeness with deep learning. *Artif. Intell. Agric.* **2020**, *4*, 31–38. [CrossRef]
48. Kirkpatrick, S.; Gelatt, C.D.; Vecchi, A. Optimization by Simulated Annealing. *Science* **1983**, *13*, 4598. [CrossRef] [PubMed]
49. Gheyas, I.A.; Smith, L.S. Feature subset selection in large dimensionality domains. *Pattern Recognit.* **2010**, *43*, 5–13. [CrossRef]
50. Pahlavani, P.; Hasanlou, M.; Nahr, S.T. Band Selection and Dimension Estimation for Hyperspectral Imagery—A New Approach Based on Invasive Weed Optimization. *J. Indian Soc. Remote Sens.* **2016**, *45*, 11–23. [CrossRef]
51. Maghsoudi, Y.; Alimohammadi, A.; Zoej, M.J.V.; Mojaradi, B. Application of Feature Selection and Classifier Ensembles for the Classification of Hyperspectral Data. In Proceedings of the 26th Asian Conference on Remote Sensing and 2nd Asian Space Conference, Hanoi, Vietnam, 7–11 November 2005; Volume 2.
52. Foody, G.M.; Mathur, A. A relative evaluation of multiclass image classification by support vector machines. *IEEE Trans. Geosci. Remote Sens.* **2004**, *42*, 1335–1343. [CrossRef]
53. Kuo, B.C.; Ho, H.H.; Li, C.H.; Hung, C.C. A Kernel-Based Feature Selection Method for SVM With RBF Kernel for Hyperspectral Image Classification. *IEEE J. Sel. Top. Appl. Earth Obs. Remote Sens.* **2013**, *7*, 317–326. [CrossRef]
54. Yang, J.; Sun, L.; Xing, W.; Feng, G.; Wang, J. Hyperspectral prediction of sugarbeet seed germination based on gauss kernel SVM. *Spectrochim. Acta Part A Mol. Biomol. Spectrosc.* **2021**, *253*, 119585. [CrossRef]
55. Pal, M.; Foody, G.M. Feature Selection for Classification of Hyperspectral Data by SVM. *IEEE Trans. Geosci. Remote Sens.* **2010**, *48*, 2297–2307. [CrossRef]
56. Wang, C.; Zhang, P.; Zhang, Y.; Zhang, L.; Wei, W. A multi-label Hyperspectral image classification method with deep learning features. In Proceedings of the International Conference on Internet Multimedia Computing and Service, Xi'an, China, 19–21 August 2016; pp. 127–131.
57. Vicente García, R.A.M.; Sánchez, J.S. Index of Balanced Accuracy: A Performance Measure for Skewed Class Distributions. In Proceedings of the 4th Iberian Conference on Pattern Recognition and Image Analysis, Povoa de Varzim, Portugal, 10–12 June 2009.
58. Gerlin, L.; Escourrou, A.; Cassan, C.; Maviane Macia, F.; Peeters, N.; Genin, S.; Baroukh, C. Unravelling physiological signatures of tomato bacterial wilt and xylem metabolites exploited by Ralstonia solanacearum. *Environ. Microbiol.* **2021**, *23*, 5962–5978. [CrossRef]
59. Lebourgeois, V.; Bégué, A.; Labbé, S.; Houlès, M.; Martiné, J. A light-weight multi-spectral aerial imaging system for nitrogen crop monitoring. *Precis. Agric.* **2012**, *13*, 525–541. [CrossRef]
60. Feifei, Y.; Shengping, L.; Yeping, Z.; Shijuan, L. Identification and level discrimination of waterlogging stress in winter wheat using hyperspectral remote sensing. *Smart Agric.* **2021**, *3*, 35. [CrossRef]
61. Kuncheva, L.I.; Faithfull, W.J. PCA feature extraction for change detection in multidimensional unlabeled data. *IEEE Trans. Neural Netw. Learn. Syst.* **2014**, *25*, 69–80. [CrossRef] [PubMed]
62. Xiao, Y.; Dong, Y.; Huang, W.; Liu, L.; Ma, H. Wheat Fusarium Head Blight Detection Using UAV-Based Spectral and Texture Features in Optimal Window Size. *Remote Sens.* **2021**, *13*, 2437. [CrossRef]
63. Khan, I.H.; Liu, H.; Li, W.; Cao, A.; Wang, X.; Liu, H.; Cheng, T.; Tian, Y.; Zhu, Y.; Cao, W.; et al. Early Detection of Powdery Mildew Disease and Accurate Quantification of Its Severity Using Hyperspectral Images in Wheat. *Remote Sens.* **2021**, *13*, 3612. [CrossRef]
64. Guo, A.; Huang, W.; Dong, Y.; Ye, H.; Ma, H.; Liu, B.; Wu, W.; Ren, Y.; Ruan, C.; Geng, Y. Wheat Yellow Rust Detection Using UAV-Based Hyperspectral Technology. *Remote Sens.* **2021**, *13*, 123. [CrossRef]